# Electronic Supplementary Information

## h*YKL-40* cancer biomarker electroanalysis in serum samples and cell lysates: capacitive immunosensing compared with enzyme label immunosorbent assays (ELISA)

W. Chaocharoen,[a,c] A. Schulte[b,c,d,*] and W. Suginta[a,c,d,*]

[a]School of Biochemistry, Institute of Science, Suranaree University of Technology, Nakhon Ratchasima, 30000, Thailand.

[b]School of Chemistry, Institute of Science, Suranaree University of Technology, Nakhon Ratchasima, 30000, Thailand.

[c]Biochemistry - Electrochemistry Research Unit, Suranaree University of Technology, Nakhon Ratchasima, 30000, Thailand.

[d]Centre of Excellence in Advanced Functional Materials, Suranaree University of Technology, Nakhon Ratchasima, 30000, Thailand.

* Correspondence to: wipa@sut.ac.th and/or schulte@sut.ac.th

**1. h*YKL-40* production with a mammalian expression system**

h*YKL-40* was produced by a transfected 293t cell line, cultured in DMEM medium. The h*YKL-40*/pCMV/hygro-His construct was generated and synthesized by a commercial supplier (Sino Biological Inc., Beijing, China). The recombinant DNA encodes the h*YKL-40* gene and an additional ten histidine residues at the C-terminus, to aid final purification of the desired protein. One day before 293t cell transfection, a cell pellet was prepared by centrifugation of a suspension at 4,500 rpm at 4 °C for 10 min, and then resuspended in 1 mL of DMEM medium without antibiotics. After a hemocytometer cell count, about 5 x $10^5$ cells were diluted into a 3-cm microtiter plate well containing 3 mL of antibiotic-free DMEM medium, followed by overnight growth in a 5% $CO_2$ incubator at 37 °C. To induce expression of h*YKL-40*, 2 µg of h*YKL-40*/pCMV/hygro-His recombinant plasmid (Sino Biological Inc., Beijing, China) were transfected by Lipofectamine® 2000. The procedure involved the addition of 6 µL of Lipofectamine® 2000 to 144 µL of antibiotic-free DMEM medium (solution 1). In parallel 2 µL of 1 µg/µL of the recombinant cDNA was pipetted into 148 µL of antibiotic-free DMEM medium and the mixture incubated for 5 min at room temperature (solution 2). The two solutions were combined and the resulting 300 µL mixture was added to the pre-prepared 293t cells, which were then allowed to grow for 48 h in a 5 % $CO_2$ incubator at 37 °C. The culture medium containing secreted h*YKL-40* was harvested and centrifuged at 4,500 rpm at 4 °C for 10 min; the cell pellet was discarded and the supernatant used for h*YKL-40* isolation and purification by affinity chromatography on a Ni-NTA agarose column run under gravity. To bind the $His_{10}$-tagged target protein, 25 µL of Ni-NTA resin, washed with equilibration buffer (50 mM $NaH_2PO_4$, 300 mM NaCl, adjusted to pH 8.0 with NaOH), was added to 10 mL of supernatant and gently shaken for 1 h at 0 °C. The resin was centrifuged at 1,000 rpm for 5 min at 4 °C, the supernatant removed and the pellet washed, first in 1 mL of equilibration buffer, followed by 1 mL of washing buffer 1 (10 mM

imidazole in equilibration buffer) and then 1 mL of washing buffer 2 (20 mM imidazole in equilibration buffer). Bound protein was eluted with 250 mM imidazole in equilibration buffer, and 1 mL fractions collected. All fractions containing h*YKL-40* were pooled and the imidazole removed and buffer exchanged to 1x PBS, pH 7.2 by dialysis (Standard RC tubing, MW cut-off 12-14 kDa, Spectrum Laboratories, Inc., CA, US). The purity of the purified h*YKL-40* protein was verified by SDS-PAGE and immunoblotting. Figure S1 shows the 12% SDS-PAGE analysis of the h*YKL-40* purification by Ni-NTA agarose. The purified protein appeared as a single band of apparent molecular weight 42 kDa (Lane 4 and 5), consistent with the expected molecular weight of 40,488 Da for h*YKL-40* without the 21- amino acid signal peptide, but with 10 additional histidine residues and N-glycosylation.

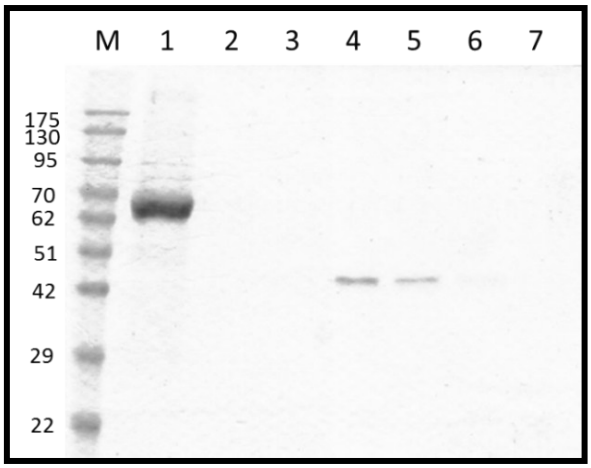


**Figure S1** 12 % SDS-PAGE analysis of Ni-NTA agarose-purified h*YKL-40* expressed in a mammalian cell line. Lane M, protein markers; lane 1, culture medium; lane 2, wash with 10 mM imidazole; lane 3, wash with 20 mM imidazole; lanes 4-7, eluate with 250 mM imidazole. Samples were loaded at 10 µL per each well.

Figure S2 shows a western blot of the purified protein, using commercial anti-h*YKL-40* (Quidel Corporation, San Diego, CA, USA); the positive band in elution fractions 1, 2 and 3 confirms the successful expression and purification. Aliquots of the purified h*YKL-40* protein were then used as the immunogen for the production of a polyclonal antibody of the protein h*YKL-40* in a 10-weeks old white New Zealand rabbit.

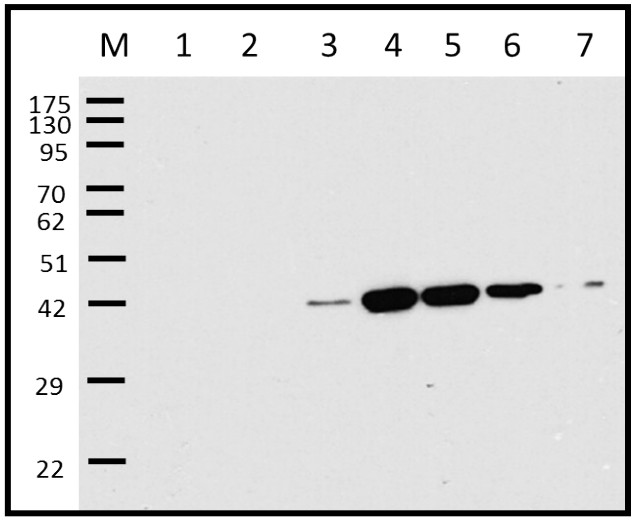


**Figure S2** h*YKL-40* detected by immunoblotting with anti-h*YKL-40*. Lane M, protein markers; lane 1, culture medium; lane 2, wash with 10 mM imidazole; lane 3, wash with 20 mM imidazole; lane 4-7, eluate with 250 mM imidazole.

## 2. Production and characterization of h*YKL-40* polyclonal antibody

Preparation of anti-h*YKL-40* followed the procedure detailed in our earlier report on h*YKL-40* immunosensing,[1] except that the immunogen was h*YKL-40* produced in a mammalian cell line, rather than in a bacterial expression system. The polyclonal anti-h*YKL-40* antiserum was first checked by 12% SDS-PAGE and western blot analysis. The in-house produced polyclonal anti-h*YKL-40* serum and commercial anti-h*YKL-40* both recognized the h*YKL-40* target protein, while no binding was detectable with the pre-immune serum (Figure S3). The 12% SDS-PAGE and western blots in Figure S4 showed that the polyclonal anti-h*YKL-40* antiserum had no affinity for the h*YKL-40* homologues h*YKL-39*, h*AMCase* and chitinase A, confirming that the polyclonal anti-h*YKL-40* had the requisite specificity for h*YKL-40* cancer biomarker detection.

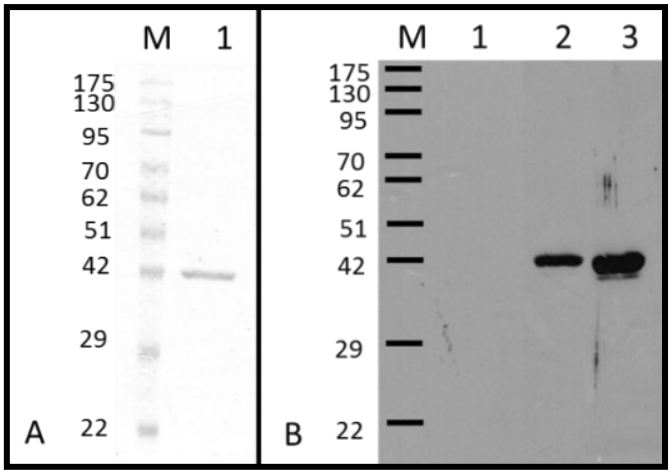


**Figure S3** Reactivity of polyclonal anti-h*YKL-40* antiserum. (A) 12% SDS-PAGE analysis of 2 μg of purified h*YKL-40*: Lane 1, Coomassie-blue stained protein. (B) Western blot Lane M, protein markers; Lane 1, pre-immune serum; Lane 2, polyclonal anti-h*YKL-40* antiserum (1:40,000 dilution); Lane 3, commercial anti-h*YKL-40* (1:10,000 dilution).

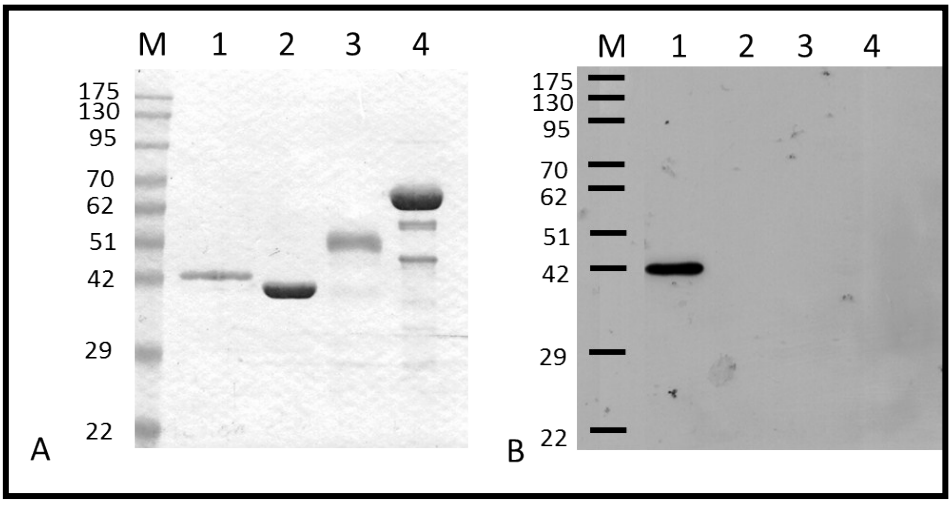


**Figure S4** Specificity of polyclonal anti-h*YKL-40* antiserum. (A) Coomassie-blue stained 12% SDS-PAGE. (B) Western blot analysis with polyclonal anti-h*YKL-40* antiserum (1:40,000 dilution); Lane 1, purified h*YKL-40* protein (2 μg); Lane 2, h*YKL-39* (3 μg); Lane 3, h*AMCase* (3 μg) and Lane 4, chitinase A (10 μg).

Polyclonal anti-h*YKL-40* antiserum was purified by affinity chromatography on a protein A agarose column run under gravity (GenScript Corporation, USA). The serum sample was diluted with binding buffer (0.15 M NaCl, 20 mM $Na_2HPO_4$, pH 8.0) at a ratio of 1:1 to ensure an optimal ionic strength and pH for binding, and further filtered through a 0.20 μm filter to remove cells. The diluted serum sample was applied under gravity to a protein A resin column, which was equilibrated with 10 column volumes of binding buffer. Bound IgG

resin was washed with 30 column volumes of binding buffer. Bound antibodies were then eluted with 10 column volumes of elution buffer (0.1 M glycine, pH 2.5), which was subsequently neutralized to pH 7.4 by addition of one tenth volume of 1 M Tris-HCl, pH 8.5. The eluted fraction was finally applied to a Hiprep 26/10 desalting column (GE-Healthcare) for exchange of buffer to 1x PBS, pH 7.2. The purity of anti-h*YKL-40* was verified by SDS-PAGE. Antibody concentration was determined with a Pierce® BCA Protein Assay kit. Purified antiserum aliquots were stored at -40 °C. SDS-PAGE analysis of the eluate (Figure S5) proved the purity of the anti-h*YKL-40* polyclonal antibody and verified that it is a protein A-specific IgG isotype. The immunoglobulin migrated above the 130 kDa marker under non-reducing conditions (Figure S5, Lane 2), while reduction of the sample led to two protein bands of about 55 and 22 kDa (Figure S5, Lane 1), as expected for IgG. Western blotting was used to determine the reactivity of purified anti-h*YKL-40*. A strong reaction with h*YKL-40* occurred at antibody concentrations down to 0.250 mg/L, whereas with the pre-immune serum no signal appeared even at the highest concentration (Figure S6).

In summary, evidence is provided that pure anti-h*YKL-40* had high specificity for h*YKL-40*, and was thus suitable as the biological recognition element of capacitive h*YKL-40* immunosensors.

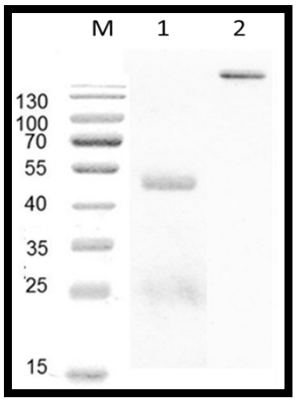


**Figure S5** Purification of anti-h*YKL-40* polyclonal antibody by protein A-agarose affinity column chromatography. 12% SDS-PAGE analysis of purified anti-h*YKL-40* polyclonal antibody; Lane 1, under reducing conditions and Lane 2, non-reducing conditions: Coomassie-blue stained gel.

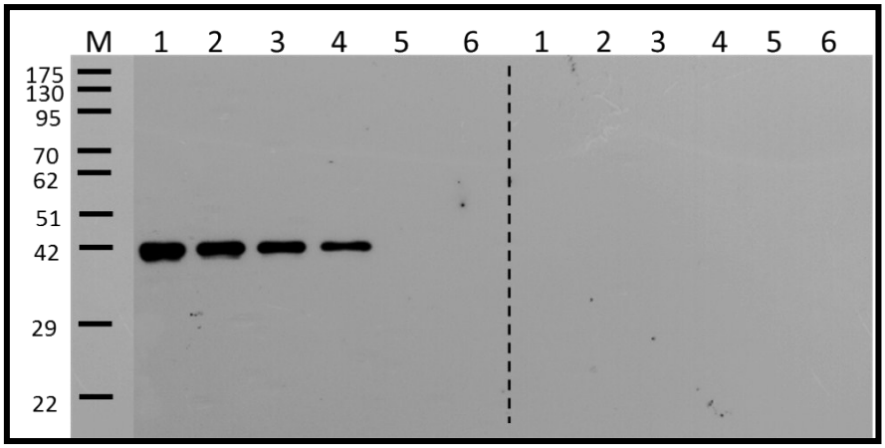


**Figure S6** Purified anti-h*YKL-40* polyclonal antibody titers against 2 µg of h*YKL-40*. Lane M, protein markers; Lane 1–6, serial dilutions of the purified antibody to 2, 1, 0.500, 0.250, 0.175 and 0.078 mg/L, respectively (left-hand panel). Unfractionated pre-immune serum was used as a negative control (right-hand panel).

**3. Gold electrode voltammetry during capacitive h*YKL-40* immunosensor preparation**

To follow the sequential chemical modification of the gold disk electrode and confirm the completion of functioning h-*YKL-40* immunosensors, cyclic voltammetry in 5 mM $K_3[Fe(CN)_6]$/0.1 M KCl was performed after each step of sensor preparation. Figure S7 shows an example of a collection of current vs. potential plots obtained at the different stages of gold electrode surface modification. At clean, smoothly polished gold electrode surfaces (black curve) the redox-active iron compound produced the expected pair of sharply peaked cathodic and anodic current waves from the faradaic reduction of Fe (III) in the forward cathodic potential scan and subsequent faradaic oxidation of Fe (II) in the reverse anodic potential scan. The size of the redox peaks decreased considerably and peak separation widened with the self-assembled thiourea film since the molecular electrode coating is non-conductive and blocks electron-transfer between dissolved species and the charged gold surface (blue curve). Reaction of glutaraldehyde with amine groups of the thiourea and subsequent covalent attachment of anti-h*YKL-40* further increased the insulation of the gold electrode, and the current was further decreased (pink and green curve, respectively). Finally, the modified electrode surface was exposed briefly to 1-dodecanethiol in order to cover any

unoccupied gold surface and establish complete insulation; the ferricyanide/ferricyanide reduction/oxidation peaks disappeared (red curve), indicating the assembly of a well-insulated h*YKL-40* modified gold surface electrode. Very thorough mechanical and electrochemical surface polishing was essential for successful capacitive immunosensor preparation. Though the smoothness and cleanness of gold disk electrodes could not be visually assessed at the end of the polishing treatment, experience ensured that most of the precursors prepared were suitable for their final application. Rare cases of unsuccessful treatment were identifiable by significant residual faradaic current activity in their ferricyanide/ferricyanide voltammograms and were rejected for use in capacitive h*YKL-40* assaying.

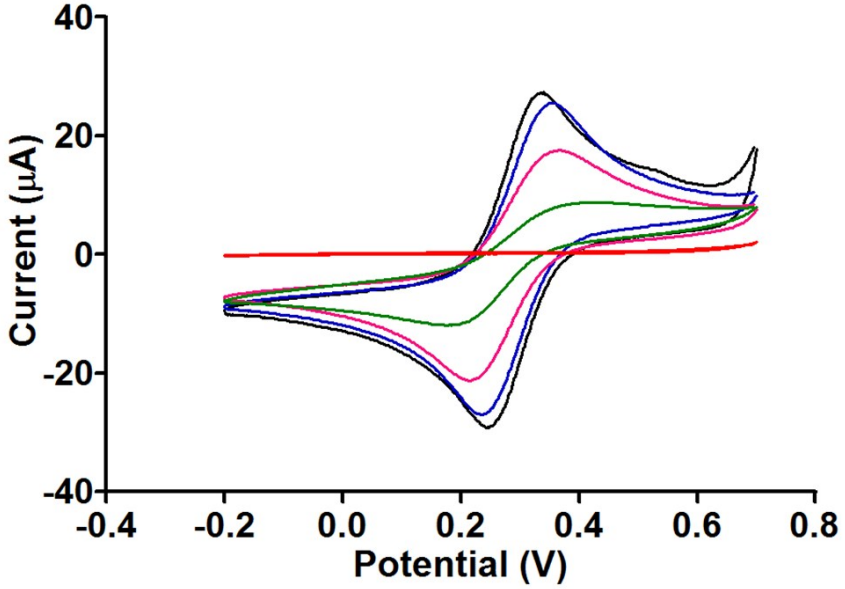


**Figure S7** Cyclic voltammograms from a gold electrode in a 5 mM $K_3[Fe(CN)_6]$/0.1 M KCl solution. Potential was measured vs. an Ag/AgCl reference electrode and the scan rate was 0.1 V/s. Black, unmodified gold electrode; blue, electrode with thiourea monolayer; pink, electrode with glutaraldehyde-modified thiourea monolayer; anti-h*YKL-40*-glutaraldehyde-thiourea electrode before (green) and after (red) final treatment with 1-dodecanethiol.

## 4. Immunosensor capacitance determination in the flow-based electrochemical system

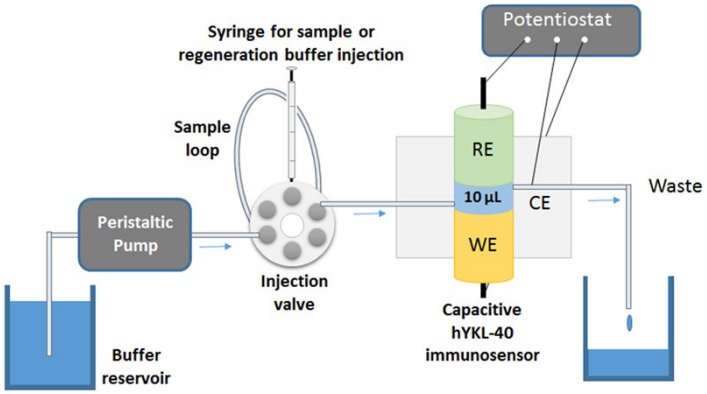


**Figure S8** Schematic of apparatus for flow-based capacitive h*YKL-40* immunosensing.

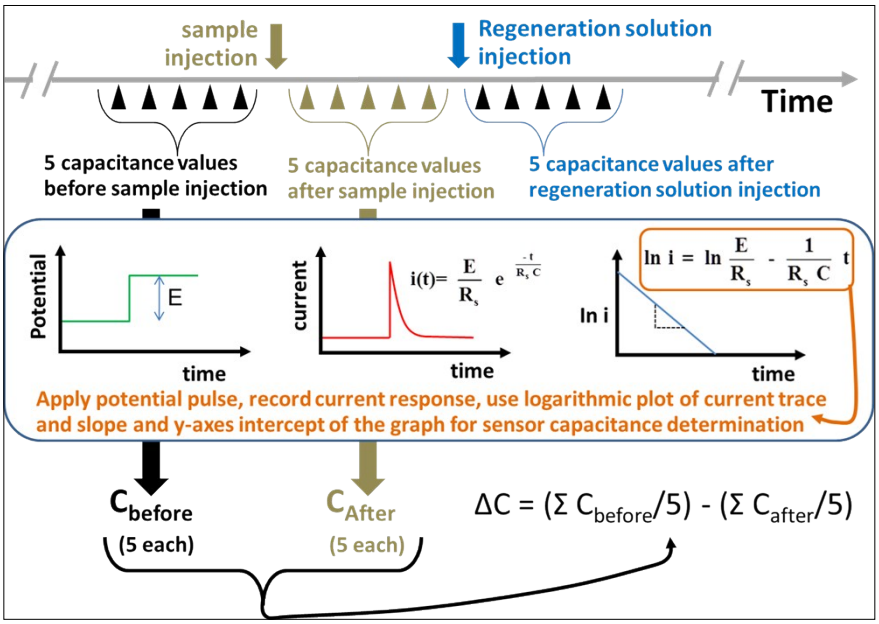


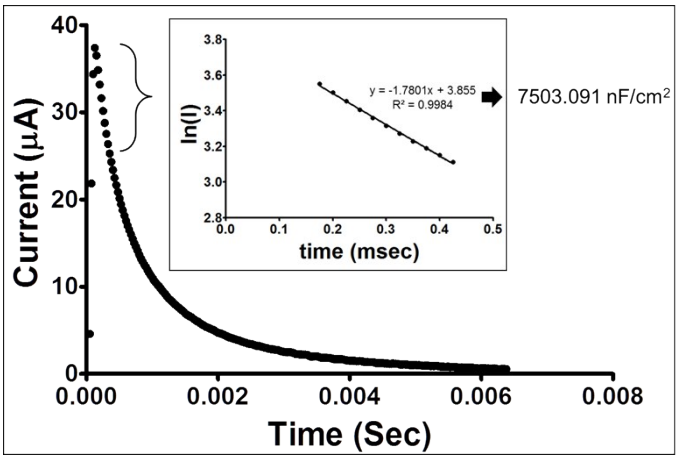


**Figure S9** Schematic illustration of h*YKL-40* immunosensor capacitance measurements by repetitive application of short potential pulses and subsequent analysis of the compilation of exponentially decaying current response (top). Example of a typical current trace as observed in response to a short 50 mV pulse to a h*YKL-40* immunosensor (bottom), with (inset) a logarithmic (ln(I) vs. time) plot.

Note that the setup for flow-based electrochemical immunosensor capacitance determinations was carefully designed for robust low-noise current measurements. For instance, the system was disconnected from the main building ground and instead directly grounded with a thick copper cable attached to a 1.5-m-long copper rod of approximately 2-cm-diameter, driven into soil. The electrical connections of the working electrode (the 'capacitive immunosensor') and the counter and reference electrodes, all prepared and maintained for optimal service, were kept as short as possible to minimize the influence of detrimental stray capacitances. A typical biomarker-signaling current recording, observed in one of the many experiments analyzed in this study, is shown as part of Figure S9. Routinely, clean and well-pronounced signal decays were observed, allowing data processing free of electrical interference.

**5. Parameter optimization for flow-based capacitive h*YKL40* immunosensing**

The type, pH and concentration of regeneration solution and running buffer, the sample volume and the flow rate for flow-based capacitive h*YKL-40* immunosensing were varied and the best values extracted, to optimize the analytical performance in biomarker detection. Evaluations of each parameter adaptation were performed in triplicate, with the other factors kept constant.

**5.1 Type and concentration of regeneration solution**

h*YKL-40* sample injection caused a change in the immunosensor capacitance as the biomarkers bound to the immobilized antibody. Subsequent injection of regeneration solution abolished the antibody/antigen interaction, allowing the captured antigen to be flushed away by the stream of buffer and returning the electrode to its original state. The criterion of successful regeneration was the fractional residual activity, % RA, of the modified electrode, which was calculated from capacitance changes induced by h*YKL-40* injections before ($\Delta C_1$) and after ($\Delta C_2$) regeneration completion as 100 x $\Delta C_2/\Delta C_1$. The regeneration solutions tested were of acidic, neutral or alkaline pH and, for the neutral solutions, varied in their ionic strength.

**Table S1:** Efficiency of h*YKL-40* removal from anti-h*YKL-40* for various regeneration solutions. Triplicate tests used 100 µL injections of 100 µg/L of h*YKL-40*.

| Regeneration solution | Average residual activity (Expressed in %) |
|---|---|
| **Low pH** | |
| 50 mM Glycine/HCl pH 2.5 | 44.5 ± 2.5 |
| 100 mM HCl (pH 1.0) | 66.8 ± 1.8 |
| 31.6 mM HCl (pH 1.5) | 73.5 ± 3.0 |
| 10 mM HCl (pH 2.0) | 81.7 ± 1.3 |
| 3.2 mM HCl (pH 2.5) | 98.2 ± 1.5 |
| 1 mM HCl (pH 3.0) | 51.5 ± 2.9 |
| **High pH** | |
| 5 mM NaOH (pH 11.7) | 40.8 ± 2.3 |
| 50 mM NaOH (pH 12.7) | 52.2 ± 2.5 |
| **High ionic strength** | |
| 1 M NaCl | 12.0 ± 2.5 |
| 1 M KCl | 28.4 ± 0.9 |
| 1 M MgCl | 24.0 ± 2.3 |

### 5.2 Optimization of type, pH and concentration of the running (flow) buffer

Phosphate, HEPES and Tris-HCl buffer solutions were tested as running buffer in the flow-based immunosensor. Phosphate buffer was chosen for subsequent work because it produced the greatest slopes of the regression lines in the region of linear response of calibration curves (i.e. the best sensitivity, Figure S10). As shown in Figure S11 and S12, the optimal pH and concentration of the phosphate buffer were pH 7.0 and 25 mM, respectively.

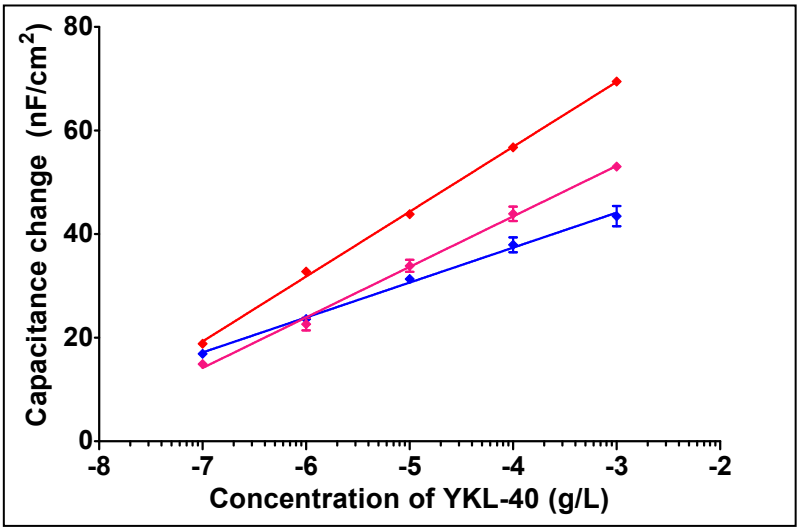


**Figure S10:** Capacitance change vs. the logarithm of h*YKL-40* for phosphate (red), HEPES (pink), and Tris-HCl (blue) running buffer solutions in the flow-based immunosensor system.

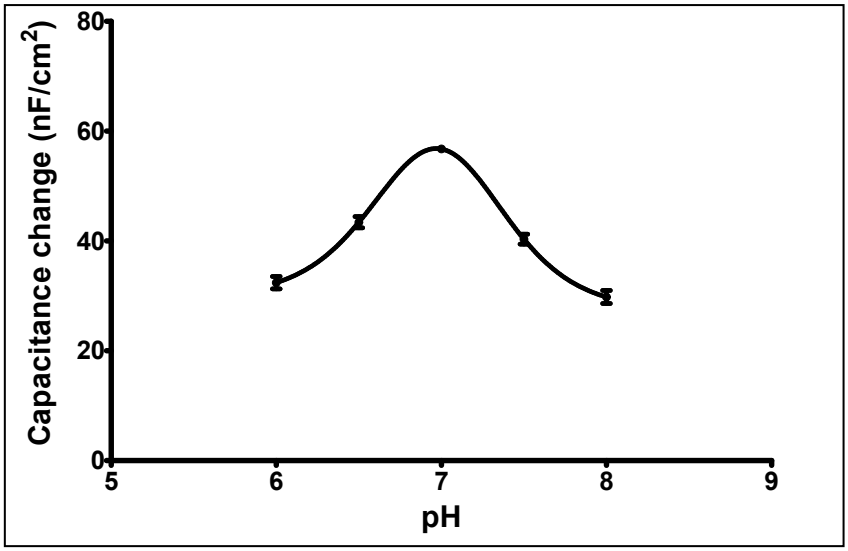


**Figure S11** Response of the immunosensor system in terms of antigen-induced immunosensor capacitance change as function of the pH of phosphate running buffer.

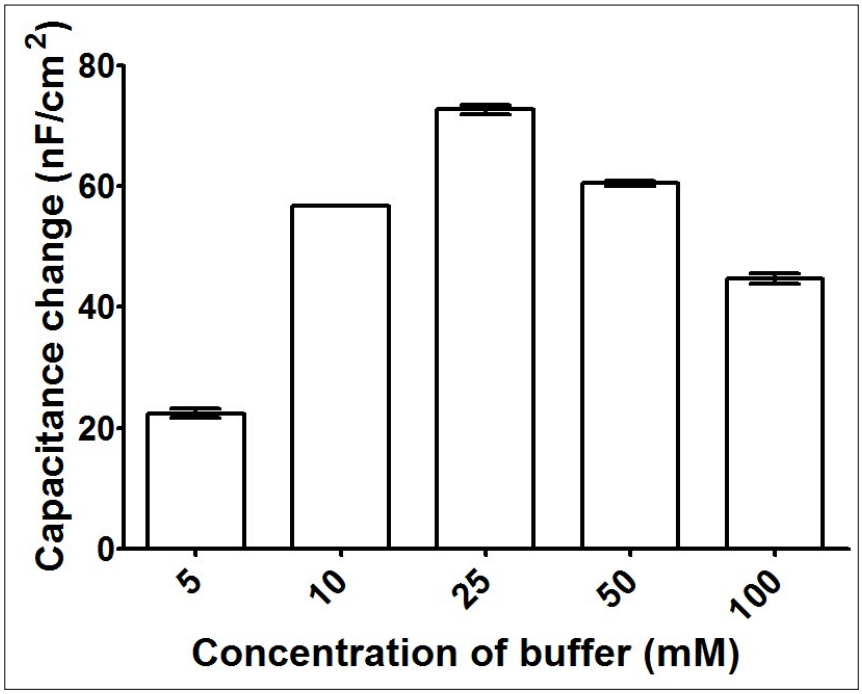


**Figure S12** Response of the immunosensor system in terms of antigen-induced immunosensor capacitance chance as function of the concentration of a pH 7.0 phosphate buffer running solution.

### 5.3 Optimization of injected sample volume and flow rate

The sample volume determines the number of molecules that can interact with immobilized antibody on the immunosensor surface and the flow rate determines the time available for the

binding process. Both had to be optimized to achieve the optimal performance of the h*YKL-40* immunosensor. As illustrated in Figure S13 an injected sample volume of 400 µL produced the largest capacitance change; however the responses with 250 and 300 µL sample injections were not significantly lower, but could be analyzed faster at a given flow rate of µL/min. 200 µL injections were chosen for quantification of h*YKL-40*, as the best compromise.

At lower flow rates the antigen has a longer time to bind to the antibody on the modified electrode, so the capacitance response increased when the flow rate was decreased (Figure S14). Of the tested flow rate values, 50 µL/min induced the highest capacitance change, closely followed by 100 µL/min. To shorten the analysis time, 100 µL/min was chosen for analytical system operation.

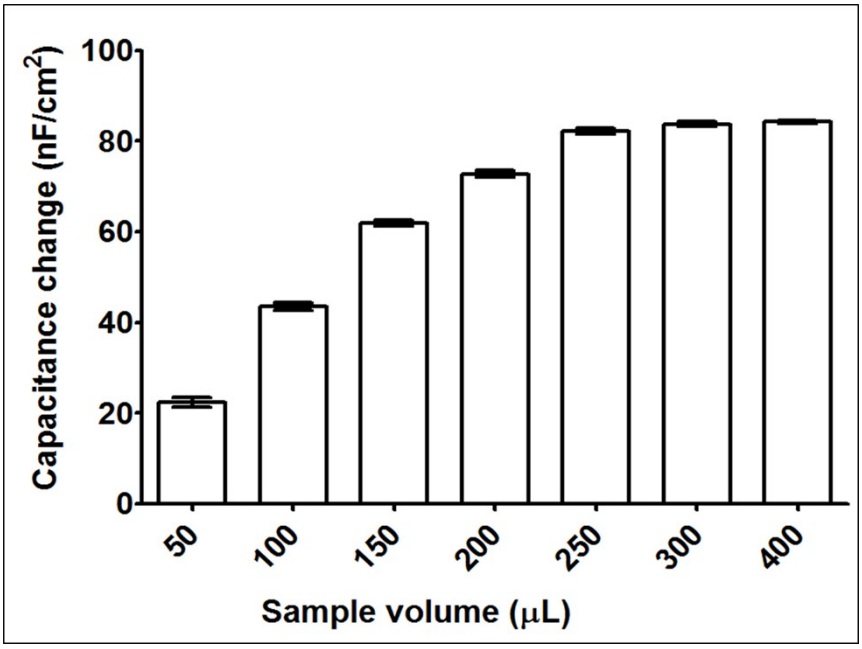


**Figure S13** Response of the immunosensor system in terms of antigen-induced immunosensor capacitance change as function of injected h*YKL-40* sample volume.

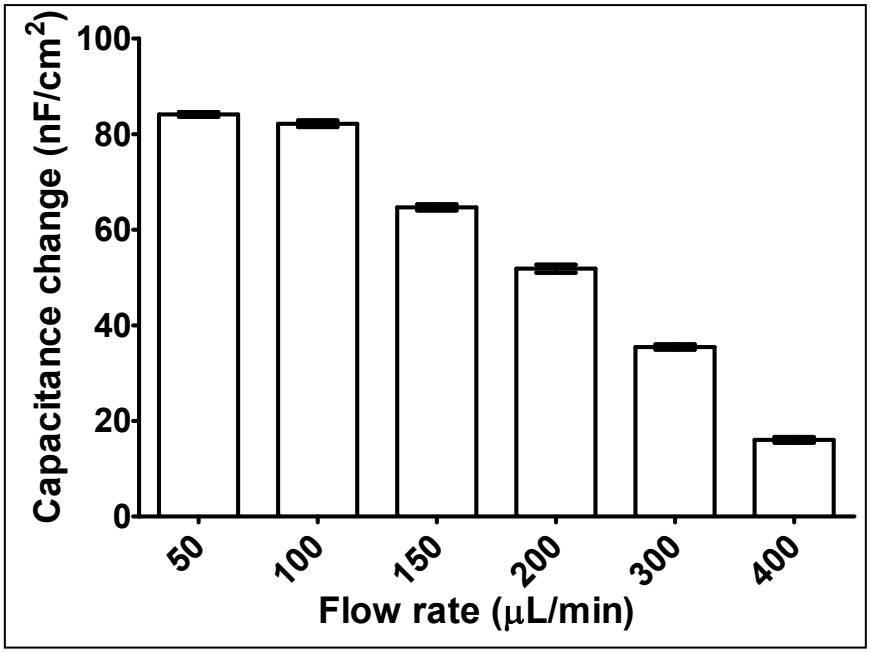


**Figure S14** Response of the immunosensor system, in terms of antigen-induced immunosensor capacitance change as a function of the flow rate of the running buffer.

### 5.4 Summary of the h*YKL-40* immunosensing parameter optimization trials

Table S2 is a summary of the above-mentioned optimization of capacitive h*YKL-40* immunosensing with specification of the optimal values for the individual influential parameters.

**Table S2:** Assayed and optimized values for flow injection-based capacitive immunosensing analysis of biomarker h*YKL-40* (3 replications)

| | **Choices** | **h*YKL-40* level (g/L)** | **Optimum** |
|---|---|---|---|
| **Buffer solutions** | | | |
| Type | 10 mM PBS[1], pH 7.0 | $10^{-7}$ to $10^{-3}$ | 10 mM PBS, pH 7.0 |
| | 10 mM HEPES[2], pH 7.0 | | |
| | 10 mM Tris[3]-HCl buffer, pH 7.0 | | |
| | | | |
| pH | 6.0, 6.5, 7.0, 7.5, 8.0 | $10^{-4}$ | 7.0 |
| | | | |
| Strength | 5, 10, 25, 50, 100 mM | $10^{-4}$ | 25 mM |
| | | | |
| **Sample volume** | | | |
| | 50, 100, 150, 200, 250, 300, 400 μL | $10^{-4}$ | 250 μL |
| | | | |
| **Flow rate** | | | |
| | 50, 100, 150, 200, 300, 400 μL/min | $10^{-4}$ | 100 μL/min |

[1]Phosphate buffer solution; [2]4-(2-hydroxyethyl)-1-piperazineethanesulfonic acid; [3]Tris(hydroxymethyl)aminomethane